TOMOGRAPHY® RESEARCH ARTICLE

Can Hyperpolarized ^{13}C-Urea be Used to Assess Glomerular Filtration Rate? A Retrospective Study

Christian Østergaard Mariager, Per Mose Nielsen, Haiyun Qi, Marie Schroeder, Lotte Bonde Bertelsen, and Christoffer Laustsen

Department of Clinical Medicine, MR Research Centre, Aarhus University, Aarhus, Denmark

Corresponding Author:
Christoffer Laustsen, PhD
Palle Juul-Jensens Boulevard 99, 8200 Aarhus N, Denmark;
E-mail: cl@clin.au.dk

Key Words: MRI, hyperpolarization, GFR

Abbreviations: Glomerular filtration rate (GFR), magnetic resonance (MR), single-kidney GFR (skGFR), dynamic contrast-enhanced (DCE), arterial input function (AIF), Baumann–Rudin (BR), ischemia-reperfusion (I/R), magnetic resonance imaging (MRI), renal blood flow (RBF)

ABSTRACT

This study investigated a simple method for calculating the single-kidney glomerular filtration rate (GFR) using dynamic hyperpolarized ^{13}C-urea magnetic resonance (MR) renography. A retrospective data analysis was applied to renal hyperpolarized ^{13}C-urea MR data acquired from control rats, prediabetic nephropathy rats, and rats in which 1 kidney was subjected to ischemia-reperfusion. Renal blood flow was determined by the model-free bolus differentiation method, GFR was determined using the Baumann–Rudin model method. Reference single-kidney and total GFRs were measured by plasma creatinine content and compared to ^{1}H dynamic contrast-enhanced estimated GFR and fluorescein isothiocyanate-inulin clearance GFR estimation. In healthy and prediabetic nephropathy rats, single-kidney hyperpolarized ^{13}C-urea GFR was estimated to be 2.5 ± 0.7 mL/min in good agreement with both gold-standard inulin clearance GFR (2.7 ± 1.2 ml/min) and ^{1}H dynamic contrast-enhanced estimated GFR (1.8 ± 0.8 mL/min), as well as plasma creatinine measurements and literature findings. Following ischemia-reperfusion, hyperpolarized ^{13}C-urea revealed a significant reduction in single-kidney GFR of 57% compared with the contralateral kidney. Hyperpolarized ^{13}C MR could be a promising tool for accurate determination of GFR. The model-free renal blood flow and arterial input function-insensitive GFR estimations are simple to implement and warrant further translational adaptation.

INTRODUCTION

Glomerular filtration rate (GFR) measures are essential to the daily care of patients, as either an estimate or an exact quantifiable measure (1). GFR is often estimated by the serum creatinine levels or creatinine clearance, derived from both blood and urine samples. Creatinine estimation is a relative insensitive marker of GFR owing to the GFR-dependent tubular secretion of creatinine (2). Inulin clearance is considered to be the most reproducible, quantitative index of renal function, as it not reabsorbed and thus transported freely to the urine. However, the specificity is lacking in both methods, as the total GFR can overshadow alterations in single kidney function or even in intrarenal differences (1).

Nuclear medicine-based techniques remain the reference method for quantification of the single-kidney GFR (skGFR) (1); widespread application of these, however, has been limited by the ionizing radiation associated with the examination. Several magnetic resonance (MR)-based methods have emerged as alternative methods to quantify skGFR. Contrast-based methods, such as dynamic contrast-enhanced (DCE) MR, have been used to generate GFR analytical models in both experimental disease and in humans (3-6). Although the methods in general show great promise, the clinical translation is lacking. This may be largely because of the lack of general consensus on model standardization, a direct consequence of the complex system in question and the obtainable signal-to-noise ratio in MR.

Recently, an alternative method for high-signal, contrast-enhanced MR has been introduced. By means of hyperpolarization of tracers containing an MR-active nucleus, the MR signal available can be enhanced by 4 orders of magnitude. In this technique, the hyperpolarized tracer itself is the origin of the signal, thereby overcoming some of the challenges associated with traditional MR contrast agents. The novel technique of hyperpolarized MR has shown applicability in a broad range of biological applications including cancer, cardiovascular, brain, liver and kidney research (7-9), with the primary goal to interrogate organ-specific metabolic substrate selection associated with various disease states (10, 11). The technique enables the

ISSN 2379-1381 http://dx.doi.org/10.18383/j.tom.2017.00010

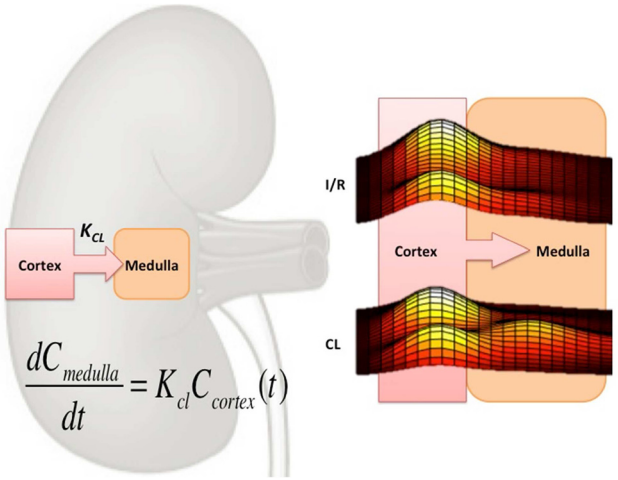

Figure 1. Illustration of the Baumann–Rudin (BR) model. Transport between the cortex to the medulla can be estimated to be a linear relationship (mass conservation). Actual line profiles of a diseased (ischemia-reperfusion [I/R]) and a healthy contralateral (CL) kidney, showing the transport from the cortical space (2 cortical peaks) to the medullary space (center peak).

important monitoring of treatment response, allowing tailored treatment planning of the individual renal patient without ionizing radiation (12-14). An increasing body of experimental evidence supports the translation of hyperpolarized MR into the clinic as a new modality for assessing renal disease (15, 12, 16-18).

In addition to metabolic imaging, several artificial or endogenous tracers have been developed for angiographic and perfusion imaging (19, 18, 5, 20-22). A tracer of particular interest is ^{13}C-urea and [^{13}C,^{15}N$_2$]urea, which is an essential osmolite associated with renal function (20). [^{13}C,^{15}N$_2$]urea possesses particular optimal properties for hyperpolarization, as the ^{15}N reduces the relaxation loss and increases the T_2 at low magnetic fields (23). Urea is vital for the kidneys' ability to concentrate urine, thereby preventing loss of water and essential nutrients (24). Urine concentration is directly determined by GFR, and thus, the intrarenal dependency of urea distribution in conjunction with renal function has previously been investigated in rodents and in porcine models with hyperpolarized ^{13}C-urea. This enables assessments of perfusion, osmolality gradients, and relaxation alterations under various functional and disease conditions (20, 23, 25-29).

Here we combine a simple, model-free analysis of renal hemodynamics and a simple, nonarterial input function (arterial input function [AIF]) GFR model, the so-called Baumann–Rudin (BR) model, on data describing the kinetics of hyperpolarized [^{13}C,^{15}N$_2$]urea handling in the rodent kidney. This indirect model of GFR assumes 2 distinct compartments—cortex and medulla; the cortex and medulla predominately contain blood and urine, respectively (Figure 1). The model assumes a unidirectional transport of contrast from the cortical space to the medullary/pelvic region. Our aim in performing this retrospective data analysis was to determine if hyperpolarized ^{13}C-urea could be used to estimate GFR in the rodent kidney.

METHODOLOGY

The data presented here were derived through retrospective analysis of hyperpolarized [^{13}C,^{15}N]urea imaging data acquired previously from the kidneys of control rats (n = 5), early diabetes rats (n = 6) (26), and ischemia-reperfusion (I/R) rats 24 hours after reperfusion (n = 6) (30). Originally, the data were analyzed to determine renal perfusion (Figure 2); here, new analytical tools were applied to extract a putative GFR based on hyperpolarized MR data (our calculated GFR will be referred to here as hGFR). To verify the findings in the previously acquired data, 9 additional animals were examined. The additional examinations include accurate hyperpolarized [^{13}C,^{15}N]-urea T_1 relaxation estimation using a single pulsed global NMR experiment (n = 4) and a gold-standard inulin clearance GFR estimation accompanying a single-kidney DCE magnetic resonance

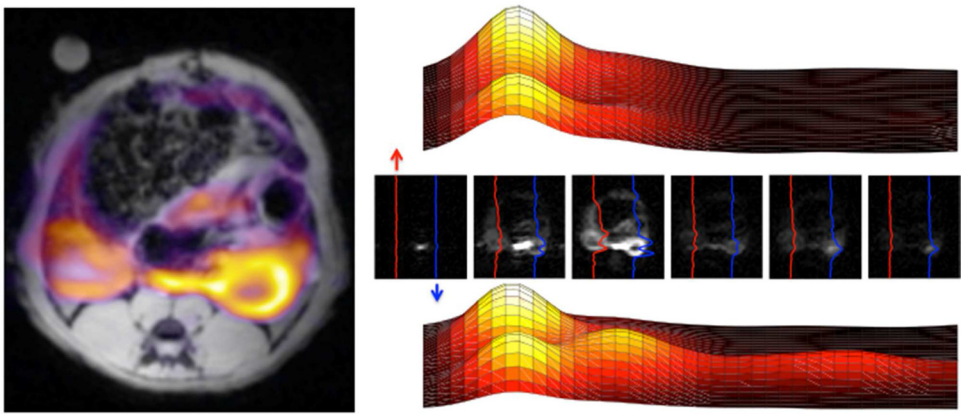

Figure 2. Anatomical T_2-weighted scan overlaid with a ^{13}C-urea image (single timepoint of 23 seconds after the start of injection) and a few selected time points illustrating the line profiles and the temporal dependencies on the distribution pattern of the hyperpolarized urea (red, left I/R kidney, blue, right contralateral kidney). Interestingly, a second peak is seen at late time points (lower line profile plot).

imaging (MRI) GFR estimation with the BR model and the model-free perfusion model (31).

Animal Handling

Experimental details have been described previously in the original perfusion imaging publications (26, 30). To summarize, [^{13}C,^{15}N]urea imaging was performed on similar conditioned female Wistar rats (220 g) 2 weeks after streptozotocin treatment (55 mg/kg) to induce a prediabetic nephropathy model (early signs of renal dysfunction, increased oxygen consumption). In similar conditioned female Wistar rats (220 g), [^{13}C,^{15}N]urea imaging was performed 24 hours after reperfusion following severe I/R injury in the left kidney (60 minutes of ischemia) (30). Additional similar conditioned 9 female Wistar rats (220 g) were anesthetized with inactin (120 mg/kg subcutaneously) for evaluation of ^{13}C global T_1, DCE skGFR, and inulin clearance.

Fluorescein Isothiocyanate-Inulin Clearance

GFR was determined using an intravenous bolus injection of fluorescein isothiocyanate (FITC)-inulin. A solution of 1.5% FITC-inulin was prepared and dialyzed (membrane molecular weight cutoff: 1000). Before injection, the FITC-inulin solution was filtered through a 0.22-μm syringe filter for sterilization. Animals were given an injection of 2 μL/kg. Further, 100 μL blood samples were collected at 1, 3, 5, 10, 15, 35, 55, and 75 minutes. Hereafter the collected plasma fractions were isolated. During the experiments, FITC-inulin were protected from light and kept on ice. Samples were diluted in 1:10 in a HEPES buffer (pH 7.4) and measured in duplicate on a 384-well plate. The original FITC-inulin solution was diluted in 1:100. Analyses were performed on a PHERAstar FS micro plate reader (Em/Ex 485 nm/520 nm; BMG Labtech, Birkerød, Denmark). FITC-inulin clearance was analyzed with a noncompartmental pharmacokinetic model (32-34).

Imaging

In both studies, a 2D fully balanced steady-state sequence with (repetition time/echo time/field of view/spectral width/matrix/section thickness of 4.8 milliseconds/2.4 milliseconds/60 × 60 mm^2/20 kHz/32 × 32/10 mm), separated by 3 seconds was used to allow perfusion assessment of the renal hemodynamics (20). The experiments were performed on a 9.4 T (Agilent, Palo Alto, California) horizontal preclinical MRI system, equipped with a ^{1}H/^{13}C Litz coil (Doty Scientific, Columbia, South Carolina) for transmission and reception. ^{1}H DCE-MRI was performed with similar experimental setup, with a standard gradient spoiled echo sequence with fat suppression (repetition time/echo time/field of view/spectral width/matrix/section thickness of 14 milliseconds/1.8 milliseconds/60 × 60 mm^2/50 kHz/128 × 128/2 mm) covering both kidneys with a temporal resolution of 1.75 seconds. Hyperpolarized [^{13}C,^{15}N$_2$]-urea T_1 relaxation estimation was performed with a dynamic series of nonselective spectroscopic acquisitions (repetition time/spectral width/flip angle of 2 seconds/20 kHz/10°).

Hyperpolarization

In both studies, a clinically ready 5 T SPINLAB polarizer was used (35). The samples was prepared by adding a mixed ratio of 200 μL of [^{13}C,^{15}N]urea (Sigma-Aldrich, Brøndby, Denmark), glycerol (Sigma-Aldrich, Brøndby, Denmark), and AH111501 (GE Healthcare, Brøndby, Denmark) (6.4 M concentration; 0.30:0.68:0.02) to a fluid path and placing it in the 5 T SPINLab polarizer (GE Healthcare, Brøndby, Denmark) for more than 2 hours to achieve a reproducible polarization of >30%. The sample was subsequently rapidly dissolved and transferred to the rats already placed in a 9.4 T preclinical MR scanner, with an injection volume of ~1.0 mL (26, 30).

Data Analysis

Renal blood flow (RBF) was estimated by using the model-free formulation by Johansson et al. (5), in which the area-under-the-curve (AUC) ratio between the AIF and the cortical tissue curve is defined as follows (in mL/min per mL cortical tissue):

$$RBF = \frac{\sum AUC_{cortex}}{\Delta t \sum AIF} \qquad (1)$$

where Δt represents the interimage delay (here 3 seconds). A correction for the plasma hematocrit, assumed to be 0.45, was used, which is similar to that used by Johansson et al. (5). Before fitting, the signal was smoothed with a lowess filter in the temporal dimension and corrected for T_1 relaxation with a T_1 relaxation time using a single exponential correction of 24 seconds (global [^{13}C,^{15}N$_2$]urea T_1 relaxation time as measured experimentally; see Results). GFR was estimated by calculating the kinetic rate (K_{cl}) of appearance of the signal in the medulla/pelvic region (36).

$$\frac{dC(t)_{medulla}}{dt} = K_{cl}\, C(t)_{cortex} \qquad (2)$$

The upslope of the curve showing [^{13}C,^{15}N]urea signal in the medulla was estimated (Figure 3), in MATLAB (The MathWorks, Inc., Natick, Massachusetts), between the initial point of the cortical slope and the peak of the medullary slope (gray area in Figure 3). GFR (estimated K_{cl}) was then obtained by dividing the medullary slope with the mean renal cortex concentration during the upslope period (37). The GFR was expressed in milliliter per minute, to allow for comparison with previously reported values for skGFR and total GFR (38). We assumed a cortical and medullary tissue density of 1 for the conversion of the perfusion and GFR values.

Statistics

Normality was assessed with quantile–quantile plots. A P-value <.05 was considered statistically significant. Statistical analysis was performed using GraphPad Prism (GraphPad Software, Inc., La Jolla, California). A 2-way paired ANOVA (left and right kidney paired) was used for statistical analysis of the renal perfusion and the GFR estimations; a post hoc Sidak multiple comparisons correction was used when appropriate. An unpaired Student t test was used for statistical analysis of the total GFR and the plasma creatinine concentration between the I/R group and the control group.

RESULTS

A [^{13}C,^{15}N]urea T_1 relaxation was found to be 24.5 ± 4 seconds (n = 4, in vivo at 9.4 T), allowing T_1 correction of the hemodynamic acquisitions. A significant renal blood flow variation was

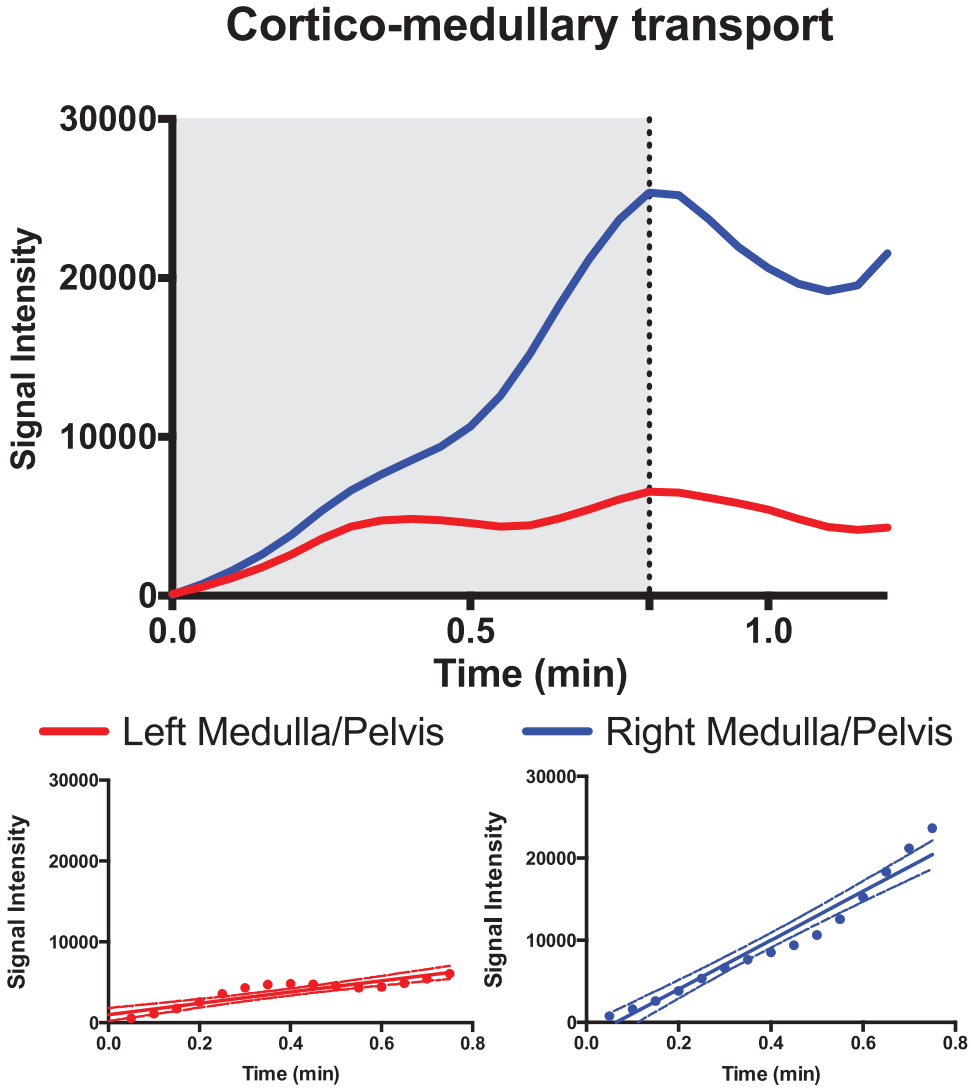

Figure 3. Region of interest (ROI) analysis signal as a function of time, showing a representative I/R (red) and contralateral (blue) medullary/pelvic signal curve. The gray area illustrates the timing to the maximum peak of the medullary signal. The bottom image shows the linear relationship between the signal intensity and the inflow over time in the medullary ROI.

observed among the 3 groups (P = .018), with a tendency toward an increased RBF in the I/R group.

No significant group difference was observed between control ^{1}H DCE-derived RBF and control hyperpolarized [^{13}C,^{15}]N-urea RBF estimations (P = .23) (Table 1). A significant variation in hGFR was observed among the individual kidneys (P = .02), with a significant difference among the groups (interaction term group × kidney, P = .02) originating from a reduction to skGFR within the I/R group with a difference of −1.6 mL/min (P = .005) between each animal's 2 kidneys. No difference was seen between the control group (P = .99) and the diabetes group (P = .99) or within these groups.

Table 1. Hemodynamic and Physiological Parameters from ^{1}H DCE and FITC-Inulin

	RBF Left Kidney	RBF Right Kidney	Body Weight	Kidney Weight	Cortical Weight	Total GFR (DCE)	GFR (inulin)
	(mL/min/mL Tissue)	(mL/min/mL Tissue)	(g)	(g)	(g)	(mL/min)	(mL/min)
1	4.02	4.71	256	0.8	0.75	5	3.8
2	4.14	3.47	235	0.75	0.7	4.7	7.3
3	6.17	5.92	266	0.8	0.72	4.4	–
4	6.78	6.99	250	0.81	0.74	1.2	8
5	3.38	1.9	222	0.68	0.58	2.3	2.3
Mean ± SD	4.9 ± 1.3	4.6 ± 1.8	245.8 ± 15.6	0.77 ± 0.05	0.7 ± 0.06	3.5 ± 1.5	5.3 ± 2.4

Abbreviations: RBF, renal blood flow; GFR, glomerular filtration rate; DCE, dynamic contrast-enhanced.

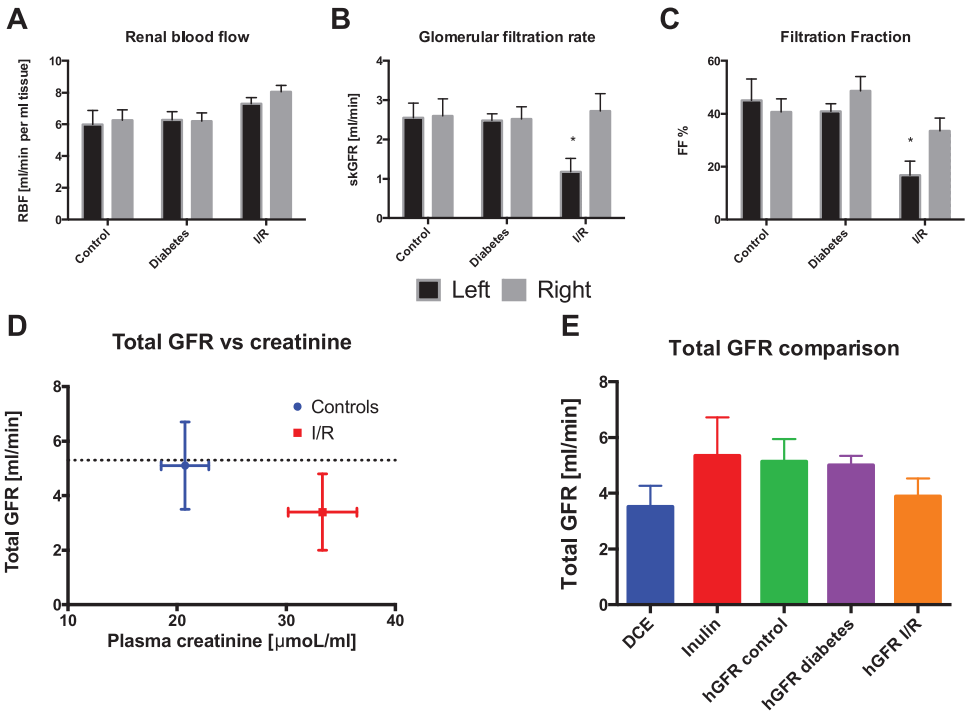

Figure 4. Renal blood flow (A), glomerular filtration (B), and filtration fraction (C), showing a clear tendency toward a general reduction in kidney function in the ischemic kidney, whereas no difference is seen between the early diabetes group and the controls. * denotes $P < .05$, mean ± SEM. Correlation between the plasma creatinine concentration and the total hGFR (sum of both kidneys) (D), showing a tendency toward decreased hGFR with increasing plasma creatinine concentrations. The lines depict the mean of the total GFR estimated with fluorescein isothiocyanate (FITC)-inulin. A comparison between the different GFR estimations shows no significant difference between the estimations with any combination of methods (E). * denotes $P < .05$ (mean ± SEM).

A filtration fraction of ≈40% was found in both early diabetic rats (44.8% ± 9.5%) and healthy controls (42.8% ± 13.7%), whereas the filtration fraction reduced in the I/R group to 25.1% ± 12.2%. To evaluate the accuracy of the GFR estimation, the MR-derived "total hGFR" (sum of both kidneys) was compared with the plasma creatinine concentration between the controls [normal animals (26) + pre-I/R (30)] of 5.1 ± 1.6 mL/min and the I/R group of 3.4 ± 1.4 mL/min (30). The total hGFR was not significantly different between the control and the I/R group (unpaired t test, $P = .28$), albeit an increased plasma creatinine concentration associated with I/R 24 hours after reperfusion was observed (unpaired t test, $P = .0045$) (Figure 4). Furthermore, no statistical significant difference was found between ^{1}H GFR and inulin measurements (paired t test, $P = .33$). In addition, no statistical difference was observed between any combinations of total GFR estimation (1-way ANOVA, $P = .4$) (Figure 4E).

DISCUSSION

The main finding in this study is the proof-of-concept that first-pass hyperpolarized [^{13}C,$^{15}N_2$]urea transport can be used to estimate GFR. GFR findings by use of hyperpolarized MR showed good agreement with gold-standard inulin clearance values and with ^{1}H DCE GFR values found under similar conditions and in congruence with previously reported values in similarly conditioned female rats, measured via the gold-standard inulin clearance (32) and with DCE-MRI (38).

Further, our estimated hGFRs compare well (1–3 mL/min lower) with human values, which are known to be on the order of 120 mL/min/70 kg, following conversion to rodent values by the allometric relationship described by Rhodin et al. (39). The allometric GFR was estimated by using the exponent range 2/3–3/4 (1.6–2.6 mL/min) (39). As previously reported (30), rats subjected to 60 min of ischemia and 24 h of reperfusion showed unaltered urine output. These data support our findings of a substantial reduction to single-kidney hGFR, whereas the total hGFR was only slightly reduced (indicated by increased plasma creatinine concentration and largely maintained hGFR, owing to residual function of the contralateral kidney). Interestingly, the data presented here suggest a compensatory effect on RBF in the contralateral kidney not subjected to I/R, although this trend did not reach significance (Figure 4). It is important to note that the inverse correlation between plasma creatinine concentration and I/R damage was not apparent in the paired experiments from the original study (30). This might be explained by the additional animals included here in the control group (n = 11) (5 from the study by Qi et al., 26, and 6 pre-IR from the study by Nielsen et al., 30) compared with the I/R group (n = 6).

Several limitations are apparent in this study. First, GFR estimation requires high spatiotemporal resolution. The interimage delay of 3 seconds reduced the accuracy of the time curve estimation and thus the fitting of the upslope of the medulla time curve. A similar effect is observed in ^{1}H GFR methods (40), and it can be largely solved by increasing the temporal resolution when acquiring the hyperpolarized images. However, the available signal must be taken into consideration, as it is limited by the hyperpolarized radio frequency (RF) signal depletion,

with a lower effective T_1 seen in the imaging section (T_{1eff} = 19 ± 3 seconds, estimated from the bSSFP images) owing to the imaging acquisition. It is difficult to compensate for the RF depletion (estimated to be 67% in these experiments; 41), as the imaging section is replenished by flowing spins into the imaging section. This is particularly important for the bolus differentiation perfusion assessment (5), potentially reducing the accuracy of the assessment, as the acquisition did not fully saturate the signal between images. The spatial resolution of 1.9 × 1.9 mm^2 is a limiting factor as well, as shown in Figure 3. Here, the medullary signal was contaminated by the cortical signal owing to partial volume effects, thereby reducing the accuracy of the method. Furthermore, it should be stressed that because of the significant reabsorption of urea, it is likely that that urea estimate GFR is apparent by nature. Furthermore, the retrospective use of data and comparison with other methods (DCE and inulin) in additional groups is a limitation of the study. Further studies are needed to fully determine the observed correlation between true GFR and the estimated hGFR.

We selected the BR model because of its ease of implementation, its lack of reliance on AIF sampling, and the need for estimating only the upslope of the signal, removing the need to sample beyond the T_1 relaxation decay. More complex models often depend on rapid and accurate sampling of the AIF and thus are particularly sensitive to appropriate placement of the imaging section and partial volumes effects of the intense signal from blood. The imaging section is typically a 1-cm mean intensity profile slab (permitted by the lack of background signal in ^{13}C MR), containing kidneys, aorta, and vena cava. However, the simplicity of the BR model also presents limitations, namely, it assumes 2 distinct separated volumes (blood and urine), when in reality, both the cortical and medullary compartments contain blood and urine (3, 36). In future, advanced AIF sampling schemes may enable the use of more sophisticated models to improve the hGFR estimation. Importantly, the current knowledge on the relaxation behavior of the hyperpolarized [^{13}C,$^{15}N_2$]urea tracer (T_1 = 24 seconds at 9.4 T) limits the correction to a global T_1 correction. In future, more appropriate relaxation models, both T_1 and T_2, could be incorporated that take compartmentalized relaxation properties into account (23, 28, 42, 43). Interestingly Reed et al. (23) have shown intrarenal compartmentalized T_2 relaxation behavior at 3 T contrary to the reported T_2 relaxation times at 9.4 T, finding only 1 T_2 component (28). This implies that this would be particularly important at 3 T and supported by using the novel T_1 and T_2 mapping sequences (23) for accurate GFR assessment.

Finally, the use of hyperpolarized [^{13}C,$^{15}N_2$]urea could potentially give rise to variations in GFR estimation, as 50% of urea is reabsorbed (24). Thus, alternative molecules such as creatinine, which are reabsorbed to a lesser degree, could potentially improve the hyperpolarized MR-based GFR estimation. Although, while typical GFR estimations are performed with free filtered-tracers (32, 2), the reabsorption of urea could represent a potential advantage over existing methods by allowing simultaneous estimation of the reabsorption (23, 25, 26, 20, 30, 29, 27). Furthermore, it has been demonstrated that several perfusion tracers can be hyperpolarized and imaged simultaneously (44), allowing more detailed knowledge on the filtration and reabsorption by combining biomarkers with different hemodynamic profiles (21, 45).

CONCLUSION

In conclusion, this study shows that hyperpolarized MR is a promising method for functional imaging of the kidneys. The study found that the estimated ^{13}C-urea GFR was in good agreement with GFR calculated from inulin clearance and DCE MRI, as well as plasma creatinine measurements and literature findings. Future work to optimize MR data acquisition schemes and to quantitatively evaluate this approach is warranted.

ACKNOWLEDGMENTS

The authors would like to acknowledge Henrik Vestergaard for laboratory assistance.

Ethical Approval: The study complied with the guidelines for use and care of laboratory animals and was approved by the Danish Inspectorate of Animal Experiments.

Disclosures: No disclosures to report.

Conflict of Interest: The authors have no conflict of interest to declare.

REFERENCES

1. Grenier N, Mendichovszky I, de Senneville BD, Roujol S, Desbarats P, Pedersen M, Wells K, Frokiaer J, Gordon I. Measurement of glomerular filtration rate with magnetic resonance imaging: principles, limitations, and expectations. Semin Nucl Med. 2008;38(1):47–55.
2. Bauer JH, Brooks CS, Burch RN. Clinical appraisal of creatinine clearance as a measurement of glomerular filtration rate. Am J Kidney Dis. 1982;2(3):337–346.
3. Annet L, Hermoye L, Peeters F, Jamar F, Dehoux JP, Van Beers BE. Glomerular filtration rate: assessment with dynamic contrast-enhanced MRI and a cortical-compartment model in the rabbit kidney. J Magn Reson Imaging. 2004;20(5):843–849.
4. Hackstein N, Heckrodt J, Rau WS. Measurement of single-kidney glomerular filtration rate using a contrast-enhanced dynamic gradient-echo sequence and the Rutland-Patlak plot technique. J Magn Reson Imaging. 2003;18(6):714–725.
5. Johansson E, Olsson LE, Månsson S, Petersson JS, Golman K, Ståhlberg F, Wirestam R. Perfusion assessment with bolus differentiation: A technique applicable to hyperpolarized tracers. Magn Reson Med. 2004;52(5):1043–1051.
6. Tofts PS, Cutajar M, Mendichovszky IA, Peters AM, Gordon I. Precise measurement of renal filtration and vascular parameters using a two-compartment model for dynamic contrast-enhanced MRI of the kidney gives realistic normal values. Eur Radiol. 2012;22(6):1320–1330.
7. Kurhanewicz J, Vigneron DB, Brindle K, Chekmenev EY, Comment A, Cunningham CH, DeBerardinis RJ, Green GG, Leach MO, Rajan SS, Rizi RR, Ross BD, Warren WS, Malloy CR. Analysis of cancer metabolism by imaging hyperpolarized nuclei: prospects for translation to clinical research. Neoplasia. 2011;13(2):81–97.
8. Rider O, Tyler D. Clinical implications of cardiac hyperpolarized magnetic resonance imaging. J Cardiovasc Magn Reson. 2013;15(1):93.
9. Laustsen C. Hyperpolarized renal magnetic resonance imaging: potential and pitfalls. Front Physiol. 2016;7:72.
10. Nelson SJ, Kurhanewicz J, Vigneron DB, Larson PEZ, Harzstark AL, Ferrone M, van Criekinge M, Chang JW, Bok R, Park I, Reed G, Carvajal L, Small EJ, Munster P, Weinberg VK, Ardenkjaer-Larsen JH, Chen AP, Hurd RE, Odegardstuen LI, Robb FJ, Tropp J, Murray JA. Metabolic imaging of patients with prostate cancer using hyperpolarized [1-13C]pyruvate. Sci Transl Med. 2013;5(198):198ra108.
11. Cunningham CH, Lau JY, Chen AP, Geraghty BJ, Perks WJ, Roifman I, Wright GA, Connelly KA. Hyperpolarized 13C metabolic MRI of the human heart: initial experience. Circ Res. 2016;119(11):1177–1182.
12. Keshari KR, Wilson DM, Sai V, Bok R, Jen KY, Larson P, Van Criekinge M, Kurhanewicz J, Wang ZJ. Noninvasive in vivo imaging of diabetes-induced renal

oxidative stress and response to therapy using hyperpolarized 13C dehydroascorbate magnetic resonance. Diabetes. 2015;64(2):344–352.
13. Laustsen C, Lipso K, Ostergaard JA, Norregaard R, Flyvbjerg A, Pedersen M, Palm F, Ardenkjaer-Larsen JH. Insufficient insulin administration to diabetic rats increases substrate utilization and maintains lactate production in the kidney. Physiol Rep. 2014;2(12):e12233.
14. Laustsen C, Nielsen PM, Nørlinger TS, Qi H, Pedersen UK, Bertelsen LB, Østergaard JA, Flyvbjerg A, Ardenkjær-Larsen JH, Palm F, Stødkilde-Jørgensen H. Antioxidant treatment attenuates lactate production in diabetic nephropathy. Am J Physiol Renal Physiol. 2016;312(1):F192–F199.
15. Laustsen C, Hansen ES, Kjaergaard U, Bertelsen LB, Ringgaard S, Stodkilde-Jorgensen H. Acute porcine renal metabolic effect of endogastric soft drink administration assessed with hyperpolarized [1-(13)C]pyruvate. Magn Reson Med. 2015;74(2):558–563.
16. Clatworthy MR, Kettunen MI, Hu D-E, Mathews RJ, Witney TH, Kennedy BWC, Bohndiek SE, Gallagher FA, Jarvis LB, Smith KGC, Brindle KM. Magnetic resonance imaging with hyperpolarized [1,4-13C2]fumarate allows detection of early renal acute tubular necrosis. Proc Natl Acad Sci U S A. 2012;109(33):13374–13379.
17. Leupold J, Månsson S, Stefan Petersson J, Hennig J, Wieben O. Fast multiecho balanced SSFP metabolite mapping of 1H and hyperpolarized 13C compounds. MAGMA. 2009;22(4):251–256.
18. Johansson E, Månsson S, Wirestam R, Svensson J, Petersson JS, Golman K, Ståhlberg F. Cerebral perfusion assessment by bolus tracking using hyperpolarized 13C. Magn Reson Med. 2004;51(3):464–472.
19. Golman K, Axelsson O, Jóhannesson H, Månsson S, Olofsson C, Petersson JS. Parahydrogen-induced polarization in imaging: subsecond 13C angiography. Magn Reson Med. 2001;46(1):1–5.
20. von Morze C, Bok RA, Sands JM, Kurhanewicz J, Vigneron DB. Monitoring urea transport in rat kidney in vivo using hyperpolarized 13C magnetic resonance imaging. Am J Physiol Renal Physiol. 2012;302(12):F1658–F1662.
21. Wigh Lipsø K, Hansen ES, Tougaard RS, Laustsen C, Ardenkjaer-Larsen JH. Renal MR angiography and perfusion in the pig using hyperpolarized water. Magn Reson Med. 2016. [Epub ahead of print]
22. von Morze C, Larson PE, Hu S, Keshari K, Wilson DM, Ardenkjaer-Larsen JH, Goga A, Bok R, Kurhanewicz J, Vigneron DB. Imaging of blood flow using hyperpolarized [(13)C]urea in preclinical cancer models. J Magn Reson Imaging. 2011;33(3):692–697.
23. Reed GD, von Morze C, Bok R, Koelsch BL, Van Criekinge M, Smith KJ, Hong S, Larson PEZ, Kurhanewicz J, Vigneron DB. High resolution (13)C MRI with hyperpolarized urea: in vivo T(2) mapping and (15)N labeling effects. IEEE Trans Med Imaging. 2014;33(2):362–371.
24. Knepper MA, Hoffert JD, Packer RK, Fenton RA. Urine concentration and dilutio. In: Brenner B, 9'th ed. The Kidney. Philadelphia, PA: Saunders Elsevier; 2008: 308–329.
25. Reed GD, von Morze C, Verkman AS, Koelsch BL, Chaumeil MM, Lustig M, Ronen SM, Bok RA, Sands JM, Larson PE, Wang ZJ, Larsen JH, Kurhanewicz J, Vigneron DB. Imaging renal urea handling in rats at millimeter resolution using hyperpolarized magnetic resonance relaxometry. Tomography. 2016;2(2):125–135.
26. Qi H, Nørlinger TS, Nielsen PM, Bertelsen LB, Mikkelsen E, Xu Y, Stødkilde Jørgensen H, Laustsen C. Early diabetic kidney maintains the corticomedullary urea and sodium gradient. Physiol Rep. 2016;4(5):e12714.
27. Bertelsen LB, Nielsen PM, Qi H, Nørlinger TS, Zhang X, Stødkilde-Jørgensen H, Laustsen C. Diabetes induced renal urea transport alterations assessed with 3D hyperpolarized 13 C,15 N-Urea. Magn Reson Med. 2016;77(4):1650–1655.
28. Laustsen C, Stokholm Nørlinger T, Christoffer Hansen D, Qi H, Mose Nielsen P, Bonde Bertelsen L, Henrik Ardenkjaer-Larsen J, Stødkilde Jørgensen H. Hyperpolarized C urea relaxation mechanism reveals renal changes in diabetic nephropathy. Magn Reson Med. 2015;75(2):515–518.
29. Hansen ES, Stewart NJ, Wild JM, Stodkilde-Jorgensen H, Laustsen C. Hyperpolarized 13 C,15 N2-urea MRI for assessment of the urea gradient in the porcine kidney. Magn Reson Med. 2016;76(6):1895–1899.
30. Nielsen PM, Szocska Hansen ES, Nørlinger TS, Nørregaard R, Bonde Bertelsen L, Stødkilde Jørgensen H, Laustsen C. Renal ischemia and reperfusion assessment with three-dimensional hyperpolarized 13 C,15 N2-urea. Magn Reson Med. 2016;76(5):1524–1530.
31. Zollner FG, Weisser G, Reich M, Kaiser S, Schoenberg SO, Sourbron SP, Schad LR. UMMPerfusion: an open source software tool towards quantitative MRI perfusion analysis in clinical routine. J Digit Imaging. 2013;26(2):344–352.
32. Fleck C. Determination of the glomerular filtration rate (GFR): methodological problems, age-dependence, consequences of various surgical interventions, and the influence of different drugs and toxic substances. Physiol Res. 1999;48(4): 267–279.
33. Qi Z, Whitt I, Mehta A, Jin J, Zhao M, Harris RC, Fogo AB, Breyer MD. Serial determination of glomerular filtration rate in conscious mice using FITC-inulin clearance. Am J Physiol Renal Physiol. 2004;286(3):F590–596.
34. Sällström J, Fridén M. Simultaneous determination of renal plasma flow and glomerular filtration rate in conscious mice using dual bolus injection. J Pharmacol Toxicol Methods. 2013;67(3):187–193.
35. Ardenkjaer-Larsen JH, Leach AM, Clarke N, Urbahn J, Anderson D, Skloss TW. Dynamic nuclear polarization polarizer for sterile use intent. NMR Biomed. 2011;24(8):927–932.
36. Baumann D, Rudin M. Quantitative assessment of rat kidney function by measuring the clearance of the contrast agent Gd(DOTA) using dynamic MRI. Magn Reson Imaging. 2000;18(5):587–595.
37. Krepkin K, Won E, Ramaswamy K, Triolo M, Stiffelma M, Rusinek H, Chandarana H. Dynamic contrast-enhanced MR renography for renal function evaluation in ureteropelvic junction obstruction: feasibility study. AJR Am J Roentgenol. 2014;202(4):778–783.
38. Zöllner FG, Schock-Kusch D, Bäcker S, Neudecker S, Gretz N, Schad LR. Simultaneous measurement of kidney function by dynamic contrast enhanced MRI and FITC-sinistrin clearance in rats at 3 tesla: initial results. PLoS One. 2013;8(11): e79992.
39. Rhodin MM, Anderson BJ, Peters AM, Coulthard MG, Wilkins B, Cole M, Chatelut E, Grubb A, Veal GJ, Keir MJ, Holford NH. Human renal function maturation: a quantitative description using weight and postmenstrual age. Pediatr Nephrol. 2009;24(1):67–76.
40. Lee VS, Rusinek H, Bokacheva L, Huang AJ, Oesingmann N, Chen Q, Kaur M, Prince K, Song T, Kramer EL, Leonard EF. Renal function measurements from MR renography and a simplified multicompartmental model. Am J Physiol Renal Physiol. 2007;292(5):F1548–F1559.
41. Laustsen C, Pileio G, Tayler MC, Brown LJ, Brown RC, Levitt MH, Ardenkjaer-Larsen JH. Hyperpolarized singlet NMR on a small animal imaging system. Magn Reson Med. 2012;68(4):1262–1265.
42. Karlsson M, Jensen PR, Ardenkjaer-Larsen JH, Lerche MH. Difference between extra- and intracellular T1 values of carboxylic acids affects the quantitative analysis of cellular kinetics by hyperpolarized NMR. Angew Chem Int Ed Engl. 2016; 55(43):13567–13570.
43. Pagès G, Puckeridge M, Liangfeng G, Tan YL, Jacob C, Garland M, Kuchel PW. Transmembrane exchange of hyperpolarized 13C-urea in human erythrocytes: subminute timescale kinetic analysis. Biophys J. 2013;105(9):1956–1966.
44. von Morze C, Bok RA, Reed GD, Ardenkjaer-Larsen JH, Kurhanewicz J, Vigneron DB. Simultaneous multiagent hyperpolarized (13)C perfusion imaging. Magn Reson Med. 2014;72(6):1599–1609.
45. Durst M, Chiavazza E, Haase A, Aime S, Schwaiger M, Schulte RF. α-trideuteromethyl[15N]glutamine: A long-lived hyperpolarized perfusion marker. Magn Reson Med. 2016;76(6):1900–1904.